Controlling the Two-Dimensional Self-Assembly of Functionalized Porphyrins via Adenine-Thymine Quartet Formation

Matthew O. Blunt, [§,*] *Ya Hu,* [§,†] *Charles W. Toft,* [‡,†] *Anna G. Slater,* [‡,†] *William Lewis,* [‡] *Neil R. Champness,* [‡,*]

[§]. The Department of Chemistry, University College London (UCL), London, WC1H 0AJ, UK

[‡]. School of Chemistry, University of Nottingham, University Park, Nottingham, NG7 2RD, UK

Corresponding Author

*E-mail: m.blunt@ucl.ac.uk; Phone: +44 207 67 91087

*E-mail: neil.champness@nottingham.ac.uk; Phone: +44 115 95 13505

ABSTRACT

The development of supramolecular synthons capable of driving hierarchical two-dimensional self-assembly is an important step towards the growth of complex and functional molecular surfaces. In this work the formation of nucleobase quartets consisting of adenine and thymine groups was used to control the 2D self-assembly of porphyrins. Tetra-(phenylthymine) zinc porphyrin (Zn-tetra-TP) and tetra-(phenyladenine) porphyrin (tetra-AP) were synthesised and scanning tunneling microscopy (STM) experiments performed to visualize their self-assembly at the liquid-solid interface between an organic solvent and a graphite surface. Mono-component solutions of both Zn-tetra-TP and tetra-AP form stable 2D structures with either thymine-thymine or adenine-adenine hydrogen bonding. Structural models based on STM data were validated using molecular mechanics (MM) simulations. In contrast, bi-component mixtures showed the formation of a structure with $p4$ symmetry consisting of alternating Zn-tetra-TP and tetra-AP molecules in a chessboard type pattern. The relative positions of the porphyrin components were identified from STM images via contrast changes associated with the zinc atom present in Zn-tetra-TP. MM simulations suggest that hydrogen bonding interactions within these structures are based on the formation of adenine-thymine (ATAT) quartets with Watson-Crick base pairing between adenine and thymine groups.

INTRODUCTION

The use of recognition interactions to control the two-dimensional (2D) self-assembly of molecules provides a route to form complex and potentially functional nanostructured surfaces.[1-3] In combination with the molecular resolution of surfaces provided by scanning tunneling microscopy (STM) this goal has been the driving force behind a wealth of research activity.[3-6] These studies use concepts from reticular synthesis[7] and molecular tectonics.[8] Rigid and planar molecular building blocks known as tectons are decorated with functional groups at specific positions. Recognition interactions between functional groups on different tectons then form supramolecular synthons[9] linking the tectons together and driving self-assembly. Coordination bonds,[10-11] halogen bonds,[12-13] van der Waals interactions,[14-15] and even dynamic covalent bond formation[15] have all been employed as recognition interactions in the growth of complex 2D molecular networks. Hydrogen bonds in particular have been widely used as stabilizing interactions for 2D self-assembly.[1, 5-6, 12] A key example of the use of hydrogen bonds as molecular recognition interactions in 2D self-assembly is the triple hydrogen bond interaction formed between perylenetetracarboxylic diimide (PTCDI) and melamine.[17-19]
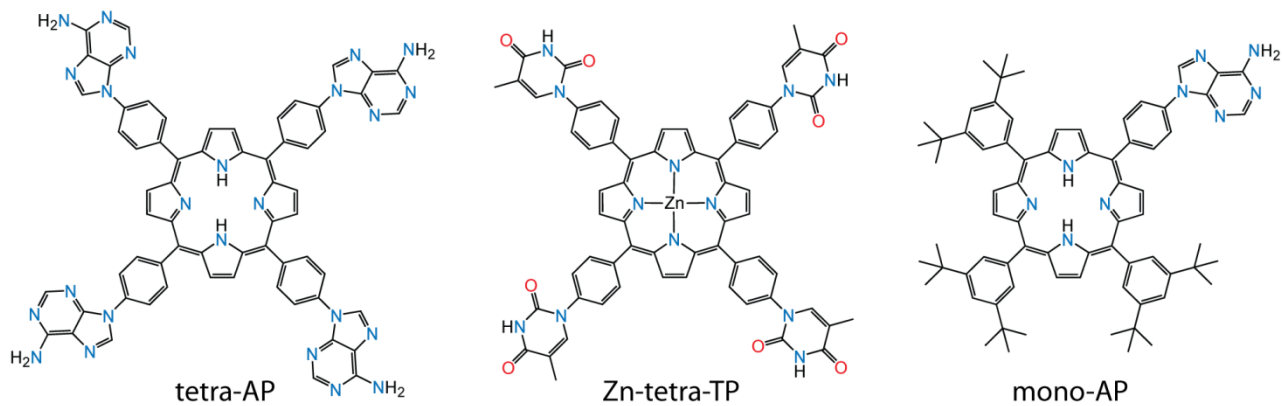
The archetypal set of supramolecular synthons based on hydrogen bonds are those formed between the nucleobases of DNA. The ability of these interactions to effect self-assembly of vastly complex biological systems makes them ideal candidates to control the formation of synthetic functional materials.[20-22] The planar structure of individual nucleobases, and of small groups of hydrogen-bonded nucleobases, means they are ideally suited to the formation of 2D molecular layers. This planarity, coupled with the strength and selectivity of their interactions has led to the 2D self-assembly of nucleobases being a widely investigated topic.[23-39] Self-assembly of the individual nucleobases adenine (A),[23-26] thymine (T),[27-28] guanine (G),[29-30] and

cytosine (C)[31] have been studied on different substrates including various coinage metals[23, 25, 28-29, 31] and graphite[24, 27, 30] and under a range of environmental conditions from ultra-high vacuum (UHV)[23, 25, 29] through to liquid-solid interfaces.[28] The 2D self-assembly of mixtures of different nucleobases has shown the formation of selective inter-nucleobase interactions but also highlighted the complexity of their hydrogen bonding landscape.[27, 32-35] The hydrogen bonding synthons observed for 2D self-assembly of nucleobases often go beyond standard Watson-Crick base pairing with a number of examples of the formation of nucleobase quartets.[33, 36-39] Guanine quartets (GGGG) occur naturally and play a key role in the structure of telomeric DNA.[40]

Through their ability to coordinate to metal ions G quartets have been the basis of novel methods for metal detection based on DNA.[41] The formation of (GGGG),[37-39] (ATAT)[33] and (GCGC)[36] quartets have all been observed via 2D self-assembly on surfaces. Despite the wealth results on mono-component or mixed nucleobase systems comparatively few studies have taken the step of using the nucleobases as functional groups to drive the 2D self-assembly of larger molecular tectons.[39, 42-46] We have previously outlined the synthesis and 2D-self-assembly of thymine functionalized porphyrins.[46] Now in this study we extend the use of nucleobase functional groups to control self-assembly by investigating bi-component mixtures of both thymine and adenine functionalized porphyrins; (Chart 1). Porphyrins are a particularly attractive choice as the basis for more complex molecular tectons and their 2D self-assembly has been widely investigated.[47] Functional groups can be included on the meso positions of a porphyrin to create tetratopic tectons. In addition to their flexibility in terms of the inclusion of peripheral functional groups, the central porphyrin macrocycle can also bind a large variety of different metal ions. Inclusion of metal ions within the porphyrin core ultimately provides a route to modify the optical, electronic and catalytic properties[48] of the resulting tectons and offers the

opportunity for additional control over self-assembly through secondary coordination to the metal.[49] Finally, in terms of self-assembly the planar nature of porphyrins promotes adsorption and ordering on surfaces while their delocalized system of π electrons and distinct cross shape makes them easily discernable in STM images.[47] The self-assembly of these nucleobase functionalized porphyrins at the liquid-solid interface between highly oriented pyrolytic graphite (HOPG) and an organic solvent layer was investigated using scanning tunneling microscopy (STM). Molecular mechanics (MM) simulations were then used in conjunction with drift corrected STM images to produce molecular models for the observed structures. Bi-component mixtures of the porphyrins demonstrated selective molecular recognition interactions in the form of unusual adenine-thymine (ATAT) quartets containing Watson-Crick hydrogen bonding between adenine and thymine groups. The formation of these nucleobase quartets resulted in a 2D molecular network consisting of the two porphyrin species arranged in an alternating chessboard type pattern.

Chart 1. Tetra-(phenylthymine) zinc porphyrin (Zn-tetra-TP) and tetra-(phenyladenine) porphyrin (tetra-AP) and model compound mono-(phenyladenine)-tri-(3,5-di-tert-butylphenyl)porphyrin (mono-A).

tetra-AP   Zn-tetra-TP   mono-AP

5

EXPERIMENTAL METHODS

    All chemical reagents were used as-purchased from Alfa Aesar, Fisher Scientific, Sigma-Aldrich, or VWR International, unless stated otherwise. Anhydrous toluene was dried by passing through a column packed with 4 Å molecular sieves, degassed and stored over a potassium mirror in a nitrogen atmosphere. Anhydrous dichloromethane was purchased from Sigma-Aldrich (Fluka) and stored over 4 Å molecular sieves. Column chromatography was performed on Merck silica gel 60 (0.2-0.5 mm, 50 - 130 mesh). Full details of the synthesis procedures and characterization details for each of the molecules discussed in the paper can be found in the ESI.

    ^{1}H and ^{13}C NMR spectra were recorded using Bruker spectrometers. EI M/S spectra were taken using a Bruker Apex IV 4.7 T mass spectrometer. MALDI-TOF M/S spectra were recorded with a Bruker Ultraflex III mass spectrometer using trans-2-[3-(4-tert-butylphenyl)-2-methyl-2-propenylidene]-malononitrile (DCTB) as the matrix. ESI M/S spectra were recorded with a Bruker MicroTOF. Single crystal X-ray diffraction experiments for mono-A and 9-propyl adenine were performed on a Rigaku Saturn724+ diffractometer equipped with a rotating anode using monochromated Cu-Kα radiation (λ = 1.5418 Å) at 120 K. The structures were solved by direct methods using either SHELXS or SHELXT[50] and refined with SHELXL[51] using a least squares method. OLEX2 software was used as the solution, refinement and analysis program.[52] All hydrogen atoms were placed in geometrically calculated positions; non-hydrogen atoms were refined with anisotropic displacement parameters.

STM experiments were performed using a Keysight Technologies 5500 STM operating in constant current mode using mechanically cut Pt:Ir (90:10) tips. Highly oriented pyrolytic graphite (HOPG) substrates (Bruker) were freshly cleaved before each experiment. Prior to deposition both the substrate and the target porphyrin solution were pre-heated to 120°C for 5 mins. A liquid cell was used to contain 25 μl of solutions on the HOPG surface. The substrate was maintained at 120°C for 5 mins following deposition before controlled cooling at 2°C min^{-1} until the sample reached room temperature. The liquid cell was covered during the cooling process to prevent evaporation. STM images were then collected at the solid-liquid interface. All STM images used to inform the construction of molecular models have been drift corrected using the underlying HOPG lattice. Full details of the STM analysis and image processing can be found in the ESI.

Molecular Mechanics (MM) and Molecular Dynamics (MD) simulations were carried out using the Forcite module in the Materials Studio 4.2 software package from Accelrys. The Dreiding force field[53] was used to assign atomic charges as well as to perform geometry optimization. A conjugate gradient algorithm was employed with an RMS force convergence parameter set to 5×10^{-3} kcal mol^{-1} Å^{-1}. The non-bonded van der Waals, and electrostatic terms both described by a cubic spline function with a cut-off at 15.5 Å and a spline width of 3 Å. Hydrogen bonding terms were described by a cubic spline function with a cut-off at 4.5 Å and a spline width of 0.5 Å. Full details of the simulations and the method used to calculate the network binding energies can be found in the ESI.
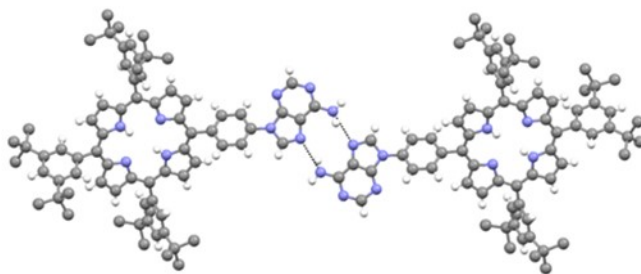
RESULTS AND DISCUSSION

The target nucleobase functionalized porphyrins were prepared by adapting our previously reported strategy for the synthesis of thymine-functionalized porphyrins.[46] The strategy requires the synthesis of a suitable aldehyde building-block which can be employed to synthesize the porphyrin. Developing our previous strategy, we prepared N-9-(4-formylphenyl)-C-6-(*bis*-boc-amino)adenine. We found it necessary to protect the adenine group using a boc-functionality[54] prior to the porphyrin forming reactions. Thus, the synthesis of N-9-(4-formylphenyl)-C-6-(*bis*-boc-amino)adenine was readily achieved from 4-formylphenylboronic acid and (*bis*-boc-amino)adenine using a Cu(OAc)$_2$-mediated Chan-Lam-Evans-modified Ullmann condensation reaction to facilitate the cross-coupling process.[55] The synthesis of the tetra-AP (Chart 1) was achieved by reaction of N-9-(4-formylphenyl)-C-6-(*bis*-boc-amino)adenine with a large excess of pyrrole using trifluoroacetic acid (TFA) to initiate the reaction, followed by oxidation with 2,3-dichloro-5,6-dicyano-1,4-benzoquinone(DDQ). Isolation of the pure target was challenging as the reaction yielded a mix of boc-protected species. TFA, required for the porphyrin synthesis, is known to lead to removal of boc groups and MALDI mass spectrometry confirmed the presence of products with loss of 0-8 boc-protecting groups. Thus, purification and isolation of a single product was difficult. To overcome this problem the range of boc-protected species were combined and the mixture treated with KOH in MeOH at 50°C. These conditions did lead to the desired product but deprotection was inefficient leading to an overall yield tetra-AP of just 2%. Tetra-AP was found to be sparingly soluble in DMSO with lower solubility in other common organic solvents, behaviour similar to that observed for tetra-TP.[44]

The synthesis of mono-AP (Chart 1) required the formation of a suitable dipyrromethene which was achieved by reaction of N-9-(4-formylphenyl)-C-6-(*bis*-boc-amino)adenine with a

large excess of pyrrole in the presence of InCl₃. The *bis*-boc-adenine functionalized

dipyrromethane was reacted with a suitable tert-butyl functionalized carbinol species, using

Lindsay's approach,[56-58] in the presence of TFA with subsequent oxidation using DDQ. The

reaction was slightly more efficient than the synthesis of tetra-AP with an 8% yield following

purification. In addition, in order to aid identification of the two similarly sized porphyrin

molecules in STM images, the zinc(II) complex of tetra-(phenylthymine) porphyrin (Zn-tetra-

TP) was prepared by simple reaction of tetra-TP[46] with zinc acetate. Further detailed information
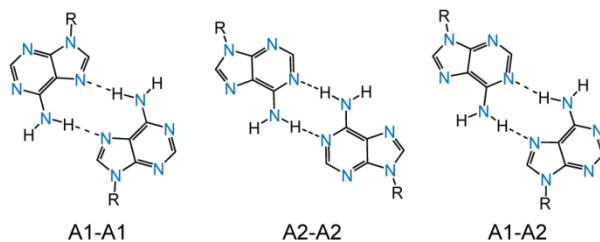
concerning synthesis is presented in the ESI.

Figure 1. The single crystal X-ray structure of mono-AP reveals an intermolecular A1-A1 arrangement in the solid-state. Nitrogen – blue; carbon – grey; hydrogen-white. Hydrogen bonds are shown by black dotted lines. EtOAc solvent molecules are omitted for clarity.

The products were characterized by conventional techniques and in the case on mono-AP by

single crystal X-ray diffraction. Slow evaporation of CDCl₃ solutions of the mono-AP,

containing small amounts of EtOAc, led to growth of single crystals of suitable quality for X-ray

diffraction studies. The X-ray structure confirms the identity of the product and the relative

arrangement of the adenine moiety with respect to the porphyrin ring (Figure 1). The structure of

mono-AP gives insight into the nature of the intermolecular interactions anticipated for adenine-

substituted porphyrin species with the most pertinent feature being the intermolecular adenine···adenine hydrogen-bonding interactions. Unfunctionalized adenine has the potential to adopt 21 different arrangements of planar hydrogen-bonded dimers, if dimers that employ C-H…N interactions are included.[59] However, functionalization at the N9 position, as employed in both mono-AP and tetra-AP, limits this number to a maximum of 15. If the steric inhibition bestowed by the large porphyrin group is considered and only stronger N-H…N interactions are used then the number of possible hydrogen-bonded dimers is further reduced to just 3 arrangements (Chart 2). Previously reported calculations suggest that the stabilization energy associated with each interaction follows a general trend of A2-A2 > A2-A1 > A1-A1, where A1 corresponds to the Hoogsteen[60] face and A2 to the Watson-Crick[61] face of adenine. A small degree of disagreement between the reported energies is found depending on the precise calculations used.[23,59,62-64] However, the single crystal structure of mono-AP, grown as an EtOAc solvate, adopts an A1-A1 intermolecular hydrogen bonding interaction. The hydrogen bond lengths [N…N = 3.084(9) Å; H…N = 2.340(9) Å; < N-H...N = 145.1(2)°] are slightly longer than those observed for the crystal structure of 9-propyl-9H-purine-6-ylamine, (9-propyladenine, see ESI) which adopts the A2-A1 interaction, or anhydrous adenine[65,66] for which two polymorphs are known which adopt either the A2-A1[65,66] interaction or both the A1-A1 and A2-A2 interactions[66] (as well as interactions involving the face of adenine that is functionalized and blocked in our systems). As the calculated differences in stabilization energy between the different intermolecular interactions is small it is possible that the arrangement observed in the structure of mono-AP is stabilized by additional hydrogen-bonding interactions to the EtOAc solvent molecules (see ESI) or that other packing interactions tip the balance in favor of the A1-A1 interaction.

Chart 2. Hydrogen-bonded adenine-adenine dimers employing solely N-H···N interactions.
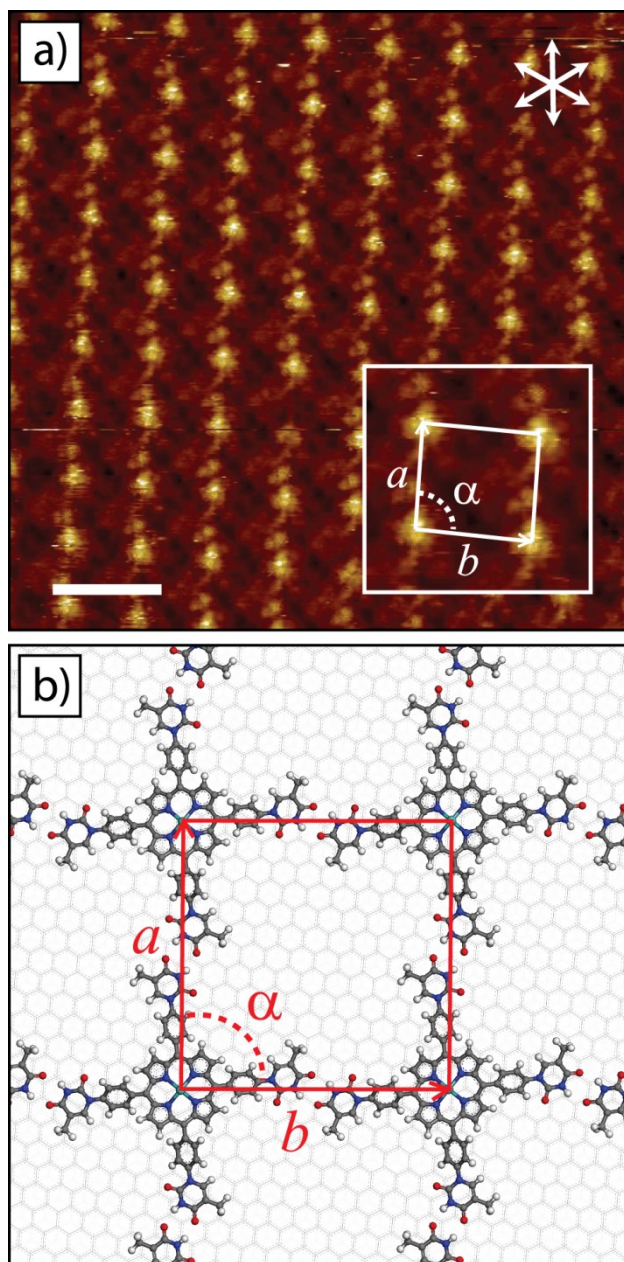

A1-A1   A2-A2   A1-A2

In addition to the structure of mono-AP we have investigated the single crystal X-ray structures of 9-propyladenine, N-1-propylthymine and a co-crystal of these two compounds (see ESI for details). As discussed above 9-propyladenine forms a hydrogen bonded arrangement which adopts an A2-A1 adenine...adenine interaction. N-1-propylthymine forms a dimeric arrangement with two thymine molecules adopting N-H…O hydrogen bonds in an $R_2^2(8)$ double hydrogen-bonded arrangement, analogous to that observed for self-assembled arrays of tetra-TP.[46] Perhaps most pertinently to this study we isolated a 1:1 co-crystal of 9-propyladenine:N-1-propylthymine which adopts a Hoogsteen hydrogen-bonding arrangement between the A1 face of the adenine moiety and thymine (see ESI).

In order to promote solubility of the nucleobase functionalized porphyrins a mixture of tetrahydrofuran (THF) and 1,2,4-trichlorobenzene (TCB) in a 1:9 volume ratio was used as a solvent. Mono-component solutions of both Zn-tetra-TP and tetra-AP were made with concentrations of ~ 4×10^{-5} M. Mixed solutions of Zn-tetra-TP and tetra-AP consisted of a 1:1 volume ratio mixture of the above solutions.

STM investigations of the self-assembly of Zn-tetra-TP (Figure 2a) show that the metallated tecton forms an identical structure to its freebase counterpart.[46] Zn-tetra-TP forms an ordered

structure on a square lattice with $p4$ symmetry that is stabilized by hydrogen bond dimers between adjacent Zn-tetra-TP molecules. The bright features observed in Figure 2a correspond to the cores of the Zn-tetra-TP molecules. Additional structure observed in the STM image is difficult to assign to a specific molecular moiety and may be the results of an imaging artefact associated with the STM tip configuration. The unit cell for the Zn-tetra-TP structure, shown in the insert to Figure 2a, has dimensions $a = (26.2 \pm 0.9)$ Å; $b = (26.3 \pm 0.5)$ Å; $\alpha = (89 \pm 2)°$ with an angle of the unit cell vectors with respect to the underlying HOPG lattice of $\theta_a = (5 \pm 2)°$ and $\theta_b = (26 \pm 2)°$. These unit cell dimensions are identical to those previously measured for freebase tetra-TP.[46] The molecular model presented in Figure 2b was produced via geometry optimized MM simulations using the unit cell dimensions from drift corrected STM images to determine the starting position / orientation of the porphyrin cores with respect to each other.

Figure 2. Self-assembly of Zn-tetra-TP at the liquid–solid interface between TCB and HOPG. **(a)** Drift corrected STM image of the Zn-tetra-TP network; bright features correspond to porphyrin cores. The insert shows a magnified view of the structure with the 2D unit cell marked. Unit cell parameters from STM are: $a = (26.2 \pm 0.9)$ Å; $b = (26.3 \pm 0.5)$ Å; $\alpha = (89 \pm 2)°$. The orientation of the underlying HOPG lattice is given by the arrows in the top right hand

corner. STM imaging parameters: V_s = -0.85 V; I_t = 10 pA. Scale bar = 4 nm. **(b)** Molecular model of the Zn-tetra-TP network from MM simulations. Unit cell parameters a = 26.7 Å; b = 26.7 Å; α = 89.4°.

Thymine groups can rotate around the bond linking them to the tetraphenyl porphyrin core. This leads to two distinct orientations that each thymine group can adopt with respect to the rest of the molecule. The orientation of the thymine groups have been selected such that the model maximizes the hydrogen bonding interactions whilst also retaining the unit cell dimensions observed via STM. In the Zn-tetra-TP molecular model shown in Figure 2b all of the thymine groups point in the same direction with respect to the porphyrin core. Unit cell dimensions from the MM simulations are a = 26.7 Å; b = 26.7 Å; α = 89.4°, with the unit cell vectors making angles with respect to the underlying HOPG lattice of θ_a = 4.6° and θ_b = 26.0°. For full details of the structures and the MM simulation procedure see the ESI.

Figure 3a shows STM images of tetra-AP self-assembled on HOPG. Cross shaped features associated with the porphyrin core are clearly visible allowing the orientation of porphyrin molecules with respect to each other to be identified. The self-assembled structure forms an oblique lattice with p2 symmetry and unit cell dimensions a = (19.8 ± 0.6) Å; b = (22.9 ± 0.7) Å; α = (84 ± 3)°. The angles of the unit cell vectors with respect to the underlying HOPG lattice are θ_a = (23 ± 4)° and θ_b = (3 ± 3)°. Figure 3b shows a suggested model for this structure based on MM simulations.
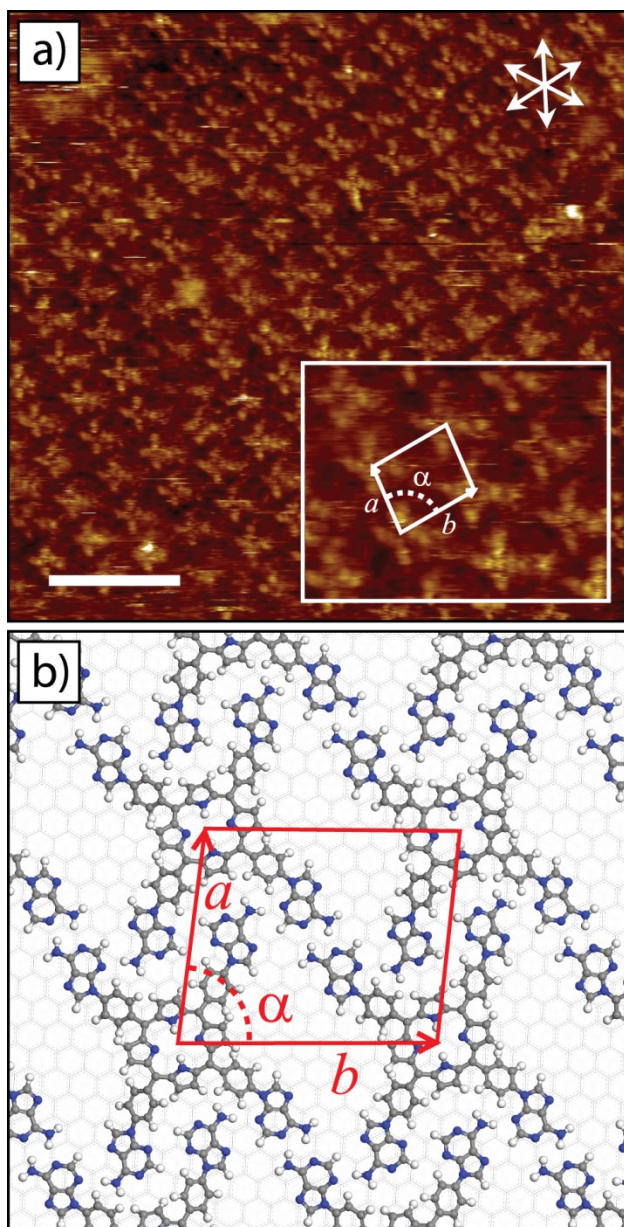
Figure 3. Self-assembly of tetra-AP at the liquid–solid interface between TCB:THF and HOPG.
(a) Drift corrected STM image of the tetra-AP network; cross shaped features correspond to the porphyrin cores. The insert shows a magnified view of the structure with the 2D unit cell marked. Unit cell parameters from STM are: $a = (19.8 \pm 0.6)$ Å; $b = (22.9 \pm 0.7)$ Å; $\alpha = (84 \pm 3)°$. The orientation of the underlying HOPG lattice is given by the arrows in the top right hand corner. STM imaging parameters: Vs = -0.65 V; It = 45 pA. Scale bar = 6 nm. **(b)** Molecular

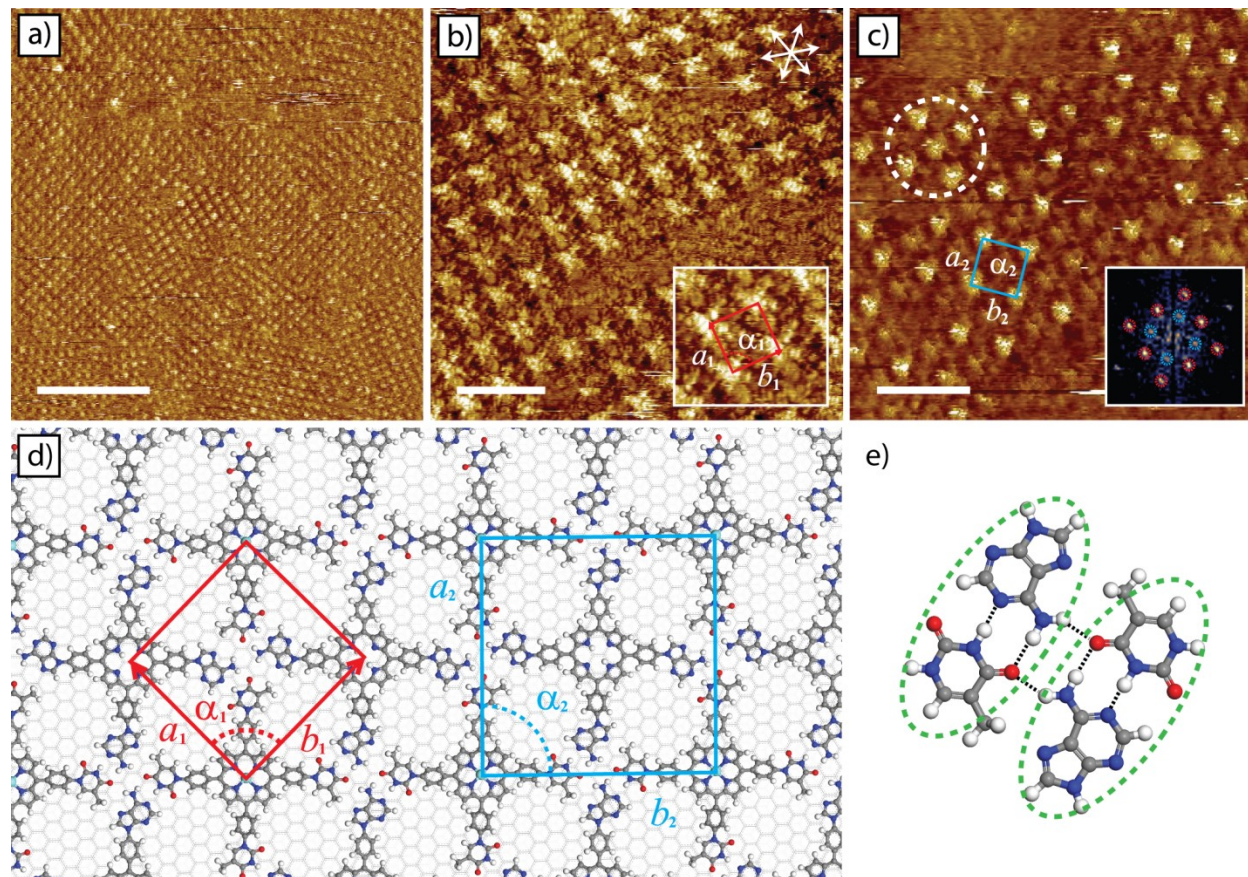model of the tetra-AP network from MM simulations. Unit cell parameters a = 19.2 Å; b = 22.8 Å; α = 83.7°.

Similar to thymine groups on Zn-tetra-TP, the adenine groups on tetra-AP can also rotate with respect to the porphyrin core allowing them to adopt two distinct orientations when the molecule is adsorbed on a surface. In contrast to Zn-tetra-TP, the adenine groups on the tetra-AP molecules shown in the model presented in Figure 3b do not all display the same orientation with respect to the porphyrin core. Instead they adopt alternating orientations around the molecule. This arrangement of the adenine groups is necessary in order to construct a molecular model that both matched the unit cell dimensions from STM measurements and produced a sensible hydrogen bonding configuration. In this model each adenine group forms three hydrogen bonds: an A2-A2 dimer formed between adenine groups on tetra-AP molecules at opposite corners of the 2D unit cell; and a third hydrogen bond formed by the close-packing of adenine groups on adjacent tetra-AP along one side of the molecule. Unit cell dimensions for the tetra-AP model from MM simulations are a = 19.2 Å; b = 22.8 Å; α = 83.7°, with the unit cell vectors making angles with respect to the underlying HOPG lattice of θ_a = 26.3° and θ_b = 2.7°.

Figure 4a-c shows examples of STM images formed by the co-deposition of 1:1 molar ratio mixtures of Zn-tetra-TP and tetra-AP on HOPG. The larger scale STM image shown in Figure 4a shows the formation of domains of ordered network between 25 and 50 nm in size. Figure 4b shows a smaller scale drift corrected STM image that shows the structure in more detail. As with Figure 4a, the cross shape of the porphyrin can be clearly seen in the image highlighting the orientation that the individual porphyrin molecules adopt. Analysis of drift corrected STM images similar to that shown in Figure 4b give unit cell dimensions (marked on Figure 4b in red)

of $a = (21.7 \pm 0.7)$ Å; $b = (22.0 \pm 0.6)$ Å; $\alpha = (90 \pm 3)°$. The angles the unit cell vectors make with respect to the underlying HOPG lattice are $\theta_a = (12 \pm 3)°$ and $\theta_b = (19 \pm 3)°$.

Figure 4. Self-assembly of Zn-tetra-TP and tetra-AP mixture. **(a)** Large scale STM image of the Zn-tetra-TP and tetra-AP network. **(b)** Drift corrected STM image of the Zn-tetra-TP and tetra-AP network; cross shaped features correspond to porphyrin cores. The insert shows a magnified view of the structure with the 2D unit cell marked in red. Unit cell parameters from STM are: $a = (21.7 \pm 0.7)$ Å; $b = (22.0 \pm 0.6)$ Å; $\alpha = (90 \pm 3)°$. The orientation of the underlying HOPG lattice is given by the arrows in the top right hand corner. **(c)** Alternate contrast image of the Zn-tetra-TP and tetra-AP network showing ordered arrangement of molecules with brighter contrast corresponding to Zn-tetra-TP; insert shows the 2D Fourier transform of the STM image. Unit

cell parameters for the marked blue cell from STM are: $a = (31.1 \pm 1.1)$ Å; $b = (30.8 \pm 1.0)$ Å; $\alpha = (90 \pm 4)°$. An example of a substitutional defect in the network, consisting of a bright Zn-tetra-TP molecule appearing in place of a darker tetra-AP molecule, is marked by the white dashed circle. STM image scale bars: **(a)** 25 nm; **(b)** 5nm and **(c)** 6 nm. STM imaging parameters: **(a)** Vs = -0.50 V, It = 10 pA; **(b)** Vs = -0.25 V, It = 10 pA; and **(c)** Vs = -0.55 V, It = 10 pA. **(d)** Molecular model of the Zn-tetra-TP and tetra-AP network from MM simulations. Unit cell parameters: red $a_1 = 21.9$ Å; $b_1 = 22.2$ Å; $\alpha_1 = 90.9°$; blue $a_2 = 31.4$ Å; $b_2 = 30.9$ Å; $\alpha_2 = 90.8°$; **(e)** Molecular model of ATAT quartet with hydrogen bonds marked as black dashed lines. AT pairs in the Watson-Crick hydrogen bonding configuration are marked by the green dashed ovals.

From Figure 4a-b it is clear that the porphyrin tectons form an ordered arrangement with the porphyrin core of each molecule in a similar orientation. By comparing both the orientation of porphyrin molecules and the STM measured unit cell dimensions to those observed for either the Zn-tetra-TP or the tetra-AP mono-component networks it is also clear that the mixed system adopts a different structure to either of the molecules on their own. However, from the STM images shown in Figure 4b it is not possible to differentiate between the Zn-tetra-TP and the tetra-AP molecules. Extended STM scanning of the network did result in occasional changes in image contrast to that seen in Figure 4c. In these images the cross shape of the porphyrin core was no longer discernable but there was a notable difference in contrast between molecules with some porphyrins appearing consistently brighter than others.

Differences in STM contrast observed for the presence or type of centrally coordinated metal ion have been widely reported previously.[67,68] The bright appearance of the central metal ion in some metal containing porphyrins, e.g. cobalt tetraphenyl porphyrin, has been linked to an orbital mediated tunneling mechanism through the partially filled dz^2 orbital on the metal ion.[68] However, although this explanation is not expected to be valid for Zn tetraphenyl porphyrin, as the dz^2 orbital is completely filled, molecular contrast in STM images is also strongly linked to the chemical nature of the STM tip apex.[69,70] Chemically modified STM tips consisting of an Au tip functionalized with thiol molecules have been used to identify the location of specific functional groups within an organic monolayer through hydrogen bond interactions.[71] A similar approach has been used by Ohshiro *et al.* to distinguish between Zn porphyrin and freebase porphyrin through coordination bonding between Zn and a pyridine functionalized STM tip.[72] While the PtIr tips used in this work have not been specifically functionalized, both porphyrin molecules can coordinate to Zn either through a carbonyl oxygen present in thymine or a pyridine-like nitrogen in adenine. Given that the STM images shown in Figure 4 were collected at the interface between HOPG and an organic solvent layer containing dissolved Zn-tetra-TP and tetra-AP it is likely that one of these molecules could adsorb at the apex of the STM tip and lead to the observed image contrast. This suggestion is consistent with the transient nature of the contrast seen in Figure 4c: adsorption or desorption of molecules from the tip apex would lead to significant changes in contrast. Additional examples of this image contrast are presented in the ESI.

Based on the observations of Ohshiro *et al.*[72] that Zn containing porphyrins appear as bright features when imaged with a pyridine functionalized tip, the brighter features in Figure 4c have been assigned as Zn-tetra-TP molecules and the dimmer features as the metal free tetra-AP

molecules. While the Zn-tetra-TP and tetra-AP network is not perfectly ordered there is a preference for the molecules to arrange in an alternating pattern. This hierarchical structure can be clearly seen in the two-dimensional Fourier transform (2DFT) shown in the insert to Figure 4c. Spots in the 2DFT have been marked with red or blue dashed circles according to the unit cell structure they originate from. The observed pattern is similar to low-energy electron diffraction (LEED) patterns obtained for a (100) surface with a $c(2\times2)$ adsorbate layer.[73]

Figure 4d shows a suggested model for this structure based on MM simulations. This structure displays $p4$ symmetry consisting of alternating Zn-tetra-TP and tetra-AP molecules arranged in a chessboard type pattern. The equivalent unit cells to those measured by STM are marked in red and blue respectively on Figure 4d. The unit cell dimensions are red: $a_1 = 21.9$ Å; $b_1 = 22.2$ Å; $\alpha_1 = 90.9°$; and blue: $a_2 = 31.4$ Å; $b_2 = 30.9$ Å; $\alpha_2 = 90.8°$. The angles that the red unit cell vectors make with respect to the underlying HOPG lattice are $\theta_a = 13.9°$ and $\theta_b = 17.0°$. These dimensions are all consistent with those obtained from drift corrected STM measurements. The structure is stabilized by hydrogen bonding in the form of adenine-thymine quartets (ATAT). These bonding arrangements form at nodal points between nucleobase functional groups from 4 adjacent porphyrin molecules. Figure 4e shows an enlarged view of one of the ATAT quartet structures. The quartet consists of two AT dimers, both in a standard Watson-Crick hydrogen bonding configuration (marked by the green dashed ovals in Figure 4e) placed next to each other. The dimers then form two additional NH$\cdots$O hydrogen bonds between amine and carbonyl groups, resulting in 6 hydrogen bonds in total for each ATAT quartet.

The formation of quartet structures has previously been observed by Mamdouh *et al.* for the 2D self-assembly of adenine and thymine on HOPG.[33] In that study DFT calculations were performed to quantify the binding energy of several different ATAT quartet structures. The

quartet structure observed in STM images by Mamdouh *et al.* consisted of a reverse Hoogsteen bonding configuration and had a calculated binding energy of E_{bind} = 1.20 eV per quartet. The quartet structure shown in Figure 4e however was calculated to have a lower binding energy of E_{bind} = 1.08 eV per quartet. While this lower binding energy suggests the arrangement in Figure 4e is not the most stable quartet structure, it is important to note that the structures studied by Mamdouh *et al.* only consisted of the nucleobase molecules without the attached porphyrins present in this study. For nucleobase functionalized porphyrins all of the planar quartet structures studied by Mamdouh *et al.*, apart from the one shown in Figure 4e, would be prevented from forming based on steric effects.[33]

Analysis of molecular dynamic (MD) quench simulations based on a previously reported method[74] was performed for the structures presented in Figures 2b, 3b and 4d in order to calculate binding energies for these structures (see ESI for full details). ‡ The binding energy values have been calculated per unit surface area to provide a more useful comparison between the different structures. The binding energies for the Zn-tetra-TP; tetra-AP; and the mixed network structures were E_{bind} = 2.04; 2.20; and 2.65 eV nm^{-2} respectively. These results would appear to validate the stabilization of the mixed network structure show in Figure 4d in comparison to either of the mono-component networks. However, the above values are calculated in the absence of solvent molecules and as such do not accurately quantify the true difference in E_{bind}. The self-assembly of nucleobase functionalized porphyrins takes place at a liquid-solid interface and therefore requires the displacement of solvent molecules from the substrate prior to formation of the network. In addition, the highly porous nature of the molecular networks described here means that co-adsorption of solvent molecules is highly likely. Both of these factors will play a significant role in determining the final binding energy. The calculations

of E_{bind} presented here include only van der Waals and hydrogen bond interactions between adjacent network molecules and between molecules and the underlying substrate. The E_{bind} values show that based only on selective hydrogen bonding interactions between nucleobase groups the mixed network has a preferential stabilization with respect to the mono-component networks. In order to obtain accurate relative binding energies of the different network structures simulations that include explicit solvent molecules would need to be performed. It should also be noted that the binding energies described above are calculated for perfectly ordered structures. From Figure 4c it is clear that there are defects present in the alternating arrangement of Zn-tetra-TP and tetra-AP molecules: *e.g.* the white dashed circle highlights a substitutional defect where a Zn-tetra-TP molecule is present where a tetra-AP is expected based on the suggested model. The presence of defects such as this will lead to the formation of different quartet structures to the one shown in Figure 4e. How the formation of these additional nucleobase quartets influences the stability of the bi-component structures requires further investigation.

CONCLUSIONS

In conclusion we have shown that selective hydrogen boding interactions between complementary nucleobase functional groups can be used to drive the hierarchical 2D self-assembly of porphyrin molecular tectons at a surface. Porphyrin tectons functionalized in the meso-positions with either T or A groups were synthesized and their 2D self-assembly at the liquid-solid interface investigated using STM and MM simulations. When mixed solutions of both A and T functionalized porphyrins were deposited at the interface a 2D molecular network was observed that is different to those formed when either of the components was deposited on

its own. By analysis of experimental data and its comparison to simulations a molecular model for the bi-component structure was suggested that consists of an alternating arrangement of A and T functionalized porphyrins in a 2D molecular networks with p4 symmetry. This network structure is stabilized via the formation of cyclic hydrogen bond configurations consisting of ATAT quartets. Formation of quartet structures is consistent both with the experimental data and represents a highly unusual observation of a nucleobase quartet structures at surfaces.[33]

The use of selective hydrogen bonding between nucleobases attached to molecular tectons represents a powerful method for the control and design of complex 2D materials. Control over the self-assembly of porphyrins, which themselves play key roles in electro-catalytic[75-77] and optoelectronic[78,79] applications, demonstrates the efficacy and potential of this approach. The formation of nucleobase quartets as the stabilizing hydrogen bond motif in these structures is also an important result and has diverse implications for nucleobase driven 2D self-assembly. These quartets share many similarities with naturally occurring "quadruplex" structures in DNA.[80] In addition to their biological functions quadruplexes also strongly coordinate to a variety of metals. This ability has seen them find application in schemes for the sensitive detection of metal-ions in solution.[41] Coordination of metal ions by surface supported G quartets on HOPG has previously been demonstrated.[81] Formation of nucleobase quartets during porphyrin self-assembly provides the possibility of multiple different metal centers, coordinated to porphyrins and quartets, arranged into hierarchically ordered surface structures. There is also the possibility that the addition of different metal ions in the presence of nucleobase functional groups could be used as a further control mechanism for the self-assembly process. Along with metal complexation by quartets, the natural extension of this work will be the synthesis and 2D self-assembly of porphyrins functionalized with G and C nucleobase groups followed by the

synthesis of asymmetrically functionalized porphyrins[82] containing different combinations of nucleobase groups within a single tecton. Using STM to perform quantitative studies of the varying roles of kinetics and thermodynamics in the self-assembly of these systems[83-86] should allow us to construct a 'tool-kit' of design principles that allow us to create new 2D molecular materials with increasing complexity and functionality.

AUTHOR INFORMATION

Corresponding Author

*E-mail: m.blunt@ucl.ac.uk; Phone: +44 207 67 91087

*E-mail: neil.champness@nottingham.ac.uk; Phone: +44 115 95 13505

Present Addresses

[†]Ya Hu: Lehn Institute of Functional Materials, MOE Laboratory of Bioinorganic and Synthetic Chemistry, Sun Yat-Sen University, Guangzhou, China.

[†]Anna G. Slater: Department of Chemistry and Materials Innovation Factory, University of Liverpool, Liverpool, L69 7ZD, UK.

[†]William Lewis: School of Chemistry, University of Sydney, NSW 2006, Australia.

Author Contributions

The manuscript was written through contributions of all authors. All authors have given approval to the final version of the manuscript.

ASSOCIATED CONTENT

Supporting Information Available: The supplementary information file (PDF) details the synthesis of the nucleobase functionalized porphyrins; single crystal X-ray structures; detailed experimental methods for the STM measurements; description of the STM drift correction and data collected from drift corrected images; details of MM and MD simulations; discussion of the calculation of binding energies based on MD simulations. This material is available free of charge via the internet at http://pubs.acs.org.

REFERENCES

(1) Bonifazi, D.; Mohnani, S.; Llanes-Pallas, A. Supramolecular Chemistry at Interfaces: Molecular Recognition on Nanopatterned Porous Surfaces. *Chem. Eur. J.* **2009,** *15* (29), 7004-7025.

(2) Slater (née Phillips), A. G.; Beton, P. H.; Champness. N. R. Two-Dimensional Supramolecular Chemistry on Surfaces. *Chem. Sci*. **2011**, *2,* 1440-1448.

(3) Sosa-Vargas, L.; Kim, E.; Attias, A. J. Beyond "Decorative" 2D Supramolecular Self-Assembly: Strategies Towards Functional Surfaces for Nanotechnology. *Mater. Horiz.* **2017,** *4* (4), 570-583.

(4) Janica, I.; Patroniak, V.; Samori, P.; Ciesielski, A. Imine-Based Architectures at Surfaces and Interfaces: From Self-Assembly to Dynamic Covalent Chemistry in 2D. *Chem. Asian J.* **2018,** *13* (5), 465-481.

(5) Mali, K. S.; Pearce, N.; De Feyter, S.; Champness, N. R. Frontiers of Supramolecular Chemistry at Solid Surfaces. *Chem. Soc. Rev.* **2017,** *46* (9), 2520-2542.

(6) Liu, L.; Xia, D.; Klausen, L. H.; Dong, M. D. The Self-Assembled Behavior of DNA Bases on the Interface. *Int. J. Mol. Sci.* **2014,** *15* (2), 1901-1914.

(7) Yaghi, O. M.; O'Keeffe, M.; Ockwig, N. W.; Chae, H. K.; Eddaoudi, M.; Kim, J. Reticular Synthesis and the Design of New Materials. *Nature* **2003,** *423* (6941), 705-714.

(8) Hosseini, M. W. Molecular Tectonics: From Simple Tectons to Complex Molecular Networks. *Acc. Chem. Res.* **2005,** *38* (4), 313-323.

(9) Desiraju, G. R. Supramolecular Synthons in Crystal Engineering - a New Organic Synthesis. *Angew. Chem. Int. Ed.* **1995,** *34* (21), 2311-2327.

(10) Adisoejoso, J.; Li, Y.; Liu, J.; Liu, P. N.; Lin, N. Two-Dimensional Metallo-Supramolecular Polymerization: Toward Size-Controlled Multi-strand Polymers. *J. Am. Chem. Soc.* **2012,** *134* (45), 18526-18529.

(11)   El Garah, M.; Ciesielski, A.; Marets, N.; Bulach, V.; Hosseini, M. W.; Samori, P. Molecular Tectonics Based Nanopatterning of Interfaces with 2D Metal-Organic Frameworks (MOFs). *Chem. Commun.* **2014,** *50* (82), 12250-12253.

(12)   Mukherjee, A.; Teyssandier, J.; Hennrich, G.; De Feyter, S.; Mali, K. S. Two-Dimensional Crystal Engineering Using Halogen and Hydrogen Bonds: Towards Structural Landscapes. *Chem. Sci.* **2017,** *8* (5), 3759-3769.

(13)   Gutzler, R.; Fu, C. Y.; Dadvand, A.; Hua, Y.; MacLeod, J. M.; Rosei, F.; Perepichka, D. F. Halogen Bonds in 2D Supramolecular Self-Assembly of Organic Semiconductors. *Nanoscale* **2012,** *4* (19), 5965-5971.

(14)   Xue, Y.; Zimmt, M. B. Patterned Monolayer Self-Assembly Programmed by Side Chain Shape: Four-Component Gratings. *J. Am. Chem. Soc.* **2012,** *134* (10), 4513-4516.

(15)   Cao, L. L.; Xu, L. R.; Zhao, D. H.; Tahara, K.; Tobe, Y.; De Feyter, S.; Lei, S. B. Efficient Molecular Recognition Based on Nonspecific Van Der Waals Interaction at the Solid/Liquid Interface. *Chem. Commun.* **2014,** *50* (80), 11946-11949.

(16)   Yue, J. Y.; Mo, Y. P.; Li, S. Y.; Dong, W. L.; Chen, T.; Wang, D. Simultaneous Construction of Two Linkages for the On-Surface Synthesis of Imine-Boroxine Hybrid Covalent Organic Frameworks. *Chem. Sci.* **2017,** *8* (3), 2169-2174.

(17)   Theobald, J. A.; Oxtoby, N. S.; Phillips, M. A.; Champness, N. R.; Beton, P. H. Controlling Molecular Deposition and Layer Structure with Supramolecular Surface Assemblies. *Nature* **2003,** *424* (6952), 1029-1031.

(18)   Raisanen, M. T.; Slater, A. G.; Champness, N. R.; Buck, M. Effects of Pore Modification on the Templating of Guest Molecules in a 2D Honeycomb Network. *Chem. Sci.* **2012,** *3* (1), 84-92.

(19)   Slater, A. G.; Perdigao, L. M. A.; Beton, P. H.; Champness, N. R. Surface-Based Supramolecular Chemistry Using Hydrogen Bonds. *Acc. Chem. Res*. **2014**, *47*, 3417−3427.

(20)   Pu, F.; Ren, J. S.; Qu, X. G. Nucleobases, Nucleosides, and Nucleotides: Versatile Biomolecules for Generating Functional Nanomaterials. *Chem. Soc. Rev.* **2018,** *47* (4), 1285-1306.

(21)   Sivakova, S.; Rowan, S. J. Nucleobases as Supramolecular Motifs. *Chem. Soc. Rev.* **2005,** *34* (1), 9-21.

(22)   Sessler, J. L.; Lawrence, C. M.; Jayawickramarajah, J. Molecular Recognition via Base-Pairing. *Chem. Soc. Rev.* **2007,** *36* (2), 314-325.

(23)   Chen, Q.; Frankel, D. J.; Richardson, N. V. Self-Assembly of Adenine on Cu(110) Surfaces. *Langmuir* **2002,** *18* (8), 3219-3225.

(24)   Freund, J. E.; Edelwirth, M.; Krobel, P.; Heckl, W. M. Structure Determination of Two-Dimensional Adenine Crystals on Graphite. *Phy. Rev. B* **1997,** *55* (8), 5394-5397.

(25)   Kelly, R. E. A.; Xu, W.; Lukas, M.; Otero, R.; Mura, M.; Lee, Y. J.; Laegsgaard, E.; Stensgaard, I.; Kantorovich, L. N.; Besenbacher, F. An Investigation into the Interactions Between Self-Assembled Adenine Molecules and a Au(111) Surface. *Small* **2008,** *4* (9), 1494-1500.

(26)   Sowerby, S. J.; Edelwirth, M.; Heckl, W. M. Self-Assembly at the Prebiotic Solid-Liquid

Interface: Structures of Self-Assembled Monolayers of Adenine and Guanine Bases Formed

on Inorganic Surfaces. *J. Phys. Chem. B* **1998,** *102* (30), 5914-5922.

(27)   Allen, M. J.; Balooch, M.; Subbiah, S.; Tench, R. J.; Balhorn, R.; Siekhaus, W. Analysis

of Adenine and Thymine Adsorbed on Graphite by Scanning Tunneling and Atomic Force

Microscopy. *Ultramicroscopy* **1992,** *42*, 1049-1053.

(28)   Roelfs, B.; Bunge, E.; Schroter, C.; Solomun, T.; Meyer, H.; Nichols, R. J.; Baumgartel,

H. Adsorption of Thymine on Gold Single-Crystal Electrodes. *J. Phys. Chem. B* **1997,** *101*

(5), 754-765.

(29)   Kong, H. H.; Sun, Q.; Wang, L. K.; Tan, Q. G.; Zhang, C.; Sheng, K.; Xu, W. Atomic-

Scale Investigation on the Facilitation and Inhibition of Guanine Tautomerization at Au(111)

Surface. *ACS Nano* **2014,** *8* (2), 1804-1808.

(30)   Srinivasan, R.; Murphy, J. C.; Fainchtein, R.; Pattabiraman, N. Electrochemical STM of

Condensed Guanine on Graphite. *J. Electroanal. Chem.* **1991,** *312* (1-2), 293-300.

(31)   Otero, R.; Lukas, M.; Kelly, R. E. A.; Xu, W.; Laegsgaard, E.; Stensgaard, I.;

Kantorovich, L. N.; Besenbacher, F. Elementary Structural Motifs in a Random Network of

Cytosine Adsorbed on a Gold(111) Surface. *Science* **2008,** *319* (5861), 312-315.

(32)   Kelly, R. E. A.; Lee, Y. J.; Kantorovich, L. N. Homopairing Possibilities of the DNA

Bases Cytosine and Guanine: An Ab-Initio DFT Study. *J. Phys. Chem. B* **2005,** *109* (46),

22045-22052.

(33)   Mamdouh, W.; Dong, M. D.; Xu, S. L.; Rauls, E.; Besenbacher, F. Supramolecular Nanopatterns Self-Assembled by Adenine-Thymine Quartets at the Liquid/Solid Interface. *J. Am. Chem. Soc.* **2006,** *128* (40), 13305-13311.

(34)   Mamdouh, W.; Kelly, R. E. A.; Dong, M. D.; Kantorovich, L. N.; Besenbacher, F. Two-Dimensional Supramolecular Nanopatterns Formed by the Coadsorption of Guanine and Uracil at the Liquid/Solid Interface. *J. Am. Chem. Soc.* **2008,** *130* (2), 695-702.

(35)   Walsh, T. R. Modelling the Nanoscale Patterning of Nucleic Acid Base Pairs Deposited on Graphite. *Mol. Phys.* **2008,** *106* (12-13), 1613-1619.

(36)   Ding, Y. Q.; Xie, L.; Zhang, C.; Xu, W. Real-Space Evidence of the Formation of the GCGC Tetrad and its Competition with the G-quartet on the Au(111) Surface. *Chem. Commun.* **2017,** *53* (71), 9846-9849.

(37)   Xu, W.; Tan, Q. G.; Yu, M.; Sun, Q.; Kong, H. H.; Laesgaard, E.; Stensgaard, I.; Kjems, J.; Wang, J. G.; Wang, C.; et al. Atomic-Scale Structures and Interactions Between the Guanine Quartet and Potassium. *Chem. Commun.* **2013,** *49* (65), 7210-7212.

(38)   Zhang, C.; Wang, L. K.; Xie, L.; Kong, H. H.; Tan, Q. G.; Cai, L. L.; Sun, Q.; Xu, W. Solventless Formation of G-Quartet Complexes Based on Alkali and Alkaline Earth Salts on Au(111). *ChemPhysChem* **2015,** *16* (10), 2099-2105.

(39)   Gonzalez-Rodriguez, D.; Janssen, P. G. A.; Martin-Rapun, R.; De Cat, I.; De Feyter, S.; Schenning, A.; Meijer, E. W. Persistent, Well-Defined, Monodisperse, pi-Conjugated Organic Nanoparticles via G-Quadruplex Self-Assembly. *J. Am. Chem. Soc.* **2010,** *132* (13), 4710-4719.

(40)   Neidle, S.; Parkinson, G. N. The Structure of Telomeric DNA. *Curr. Opin. Struct. Biol.* **2003,** *13* (3), 275-283.

(41)   Zhou, W. H.; Saran, R.; Liu, J. W. Metal Sensing by DNA. *Chem. Rev.* **2017,** *117* (12), 8272-8325.

(42)   Tan, Q. G.; Zhang, C.; Wang, N.; Zhu, X. J.; Sun, Q.; Jacobsen, M. F.; Gothelf, K. V.; Besenbacher, F.; Hu, A. G.; Xu, W. Tailoring On-Surface Supramolecular Architectures Based on Adenine Directed Self-Assembly. *Chem. Commun.* **2014,** *50* (3), 356-358.

(43)   Chng, G. Y. Y.; Sun, X.; Cho, S. J.; Rajwar, D.; Grimsdale, A. C.; Fichou, D. Synthesis and 2D Self-Assembly at the Liquid-Solid Interface of Novel H-bonding Linear Pi-Conjugated Oligomers Terminated by Uracil and Melamine Units. *New J. Chem.* **2014,** *38* (6), 2407-2413.

(44)   Llanes-Pallas, A.; Palma, C. A.; Piot, L.; Belbakra, A.; Listorti, A.; Prato, M.; Samori, P.; Armaroli, N.; Bonifazi, D. Engineering of Supramolecular H-Bonded Nanopolygons via Self-Assembly of Programmed Molecular Modules. *J. Am. Chem. Soc.* **2009,** *131* (2), 509-520.

(45)   Palma, C. A.; Bjork, J.; Bonini, M.; Dyer, M. S.; Llanes-Pallas, A.; Bonifazi, D.; Persson, M.; Samori, P. Tailoring Bicomponent Supramolecular Nanoporous Networks: Phase Segregation, Polymorphism, and Glasses at the Solid-Liquid Interface. *J. Am. Chem. Soc.* **2009,** *131* (36), 13062-13071.

(46)   Slater, A. G.; Hu, Y.; Yang, L. X.; Argent, S. P.; Lewis, W.; Blunt, M. O.; Champness, N. R. Thymine Functionalised Porphyrins, Synthesis and Heteromolecular Surface-Based Self-Assembly. *Chem Sci* **2015,** *6* (2), 1562-1569.

(47)   Otsuki, J. STM Studies on Porphyrins. *Coord. Chem. Rev.* **2010,** *254* (19-20), 2311-2341.

(48)   Hulsken, B.; Van Hameren, R.; Gerritsen, J. W.; Khoury, T.; Thordarson, P.; Crossley, M. J.; Rowan, A. E.; Nolte, R. J. M.; Elemans, J.; Speller, S. Real-Time Single-Molecule Imaging of Oxidation Catalysis at a Liquid-Solid Interface. *Nat. Nanotechnol.* **2007,** *2* (5), 285-289.

(49)   Visser, J.; Katsonis, N.; Vicario, J.; Feringa, B. L. Two-Dimensional Molecular Patterning by Surface-Enhanced Zn-Porphyrin Coordination. *Langmuir* **2009,** *25* (10), 5980-5985.

(50)   Sheldrick, G. SHELXT - Integrated Space-Group and Crystal-Structure Determination. *Acta Cryst. A* **2015**, 71, 3-8.

(51)   Sheldrick, G. Crystal Structure Refinement with SHELXL. *Acta Cryst. C* **2015**, 71, 3-8.

(52)   Dolomanov, O. V.; Bourhis, L. J.; Gildea, R. J.; Howard, J. A. K.; Puschmann, H. OLEX2: a Complete Structure Solution, Refinement and Analysis Program. *J. Appl. Cryst*. **2009**, 42, 339-341.

(53)   Mayo, S. L.; Olafson, B. D.; Goddard, W. A., III. Dreiding - a Generic Force-Field for Molecular Simulations. *J. Phys. Chem.* **1990**, 94, 8897-8909.

(54)   Dey, S.; Garner, P. Synthesis of Tert-Butoxycarbonyl (Boc)-Protected Purines. *J. Org. Chem.* **2000**, *65*, 7697-7699.

(55)   Jacobsen, M. F.; Knudsen, M. M.; Gothelf, K. V. Efficient N-Arylation and N-Alkenylation of the Five DNA/RNA Nucleobases. *J. Org. Chem.* **2006**, *71*, 9183-9190.

(56)   Lee, C.-H.; Li, F.; Iwamoto, K.; Dadok, J.; Bothner-By, A. A.; Lindsey, J. S. Synthetic Approaches to Regioisomerically Pure Porphyrins Bearing 4 Different Mesosubstituents. *Tetrahedron* **1995**, *51*, 11645–11672.

(57)   Rao, P. D.; Dhanalekshmi, S.; Littler B. J.; Lindsey, J. S. Rational Syntheses of Porphyrins Bearing up to Four Different Meso Substituents. *J. Org. Chem.* **2000**, *65*, 7323–7344.

(58)   Rao, P. D.; Littler, B. J.; Geier III, G. R.; Lindsey, J. S. Efficient Synthesis of Monoacyl Dipyrromethanes and Their Use in the Preparation of Sterically Unhindered Trans-Porphyrins. *J. Org. Chem.* **2000**, *65*, 1084–1092.

(59)   Kelly, R. E. A.; Lee, Y. J.; Kantorovich, L. N. Homopairing Possibilities of the DNA Base Adenine. *J. Phys. Chem. B*. **2005**, *109*, 11933-11939.

(60)   Hoogsteen, K. Crystal and Molecular Structure of a Hydrogen-Bonded Complex between 1-Methylthymine and 9-Methyladenine. *Acta Cryst.* **1963**, *16*, 907–916.

(61)   Watson, J. D.; Crick, F. H. C. Molecular Structure of Nucleic Acids - a Structure for Deoxyribose Nucleic Acid. *Nature* **1953**, *171*, 737-738.

(62)   Furukawa, M.; Tanaka, H.; Kawai, T. The Role of Dimer Formation in the Self-Assemblies of DNA Base Molecules on Cu(111) Surfaces: A Scanning Tunneling Microscope Study. *J. Chem. Phys*. **2001**, *115*, 3419-3423.

(63)   Edelwirth, M.; Freund, J., Sowerby, S. J.; Heckl, W. M. Molecular Mechanics Study of Hydrogen Bonded Self-Assembled Adenine Monolayers on Graphite. *Surf. Sci*. **1998**, *417*, 201-209.

(64)   Sponer, J.; Jurecka, P.; Hobza, P. Accurate Interaction Energies of Hydrogen-Bonded Nucleic Acid Base Pairs. *J. Am. Chem. Soc*. **2004**, *126*, 10142-10151.

(65)   Mahapatra, S.; Nayak, S. K.; Prathapa, S. J.; Guru Row, T.N. Anhydrous Adenine: Crystallization, Structure, and Correlation with Other Nucleobases. *Crystal Growth Des*. **2008**, *8*, 1223-1225.

(66)   Stolar, T.; Lukin, S.; Požar, J.; Rubčić, M.; Day, G. M.; Biljan, I.; Jung, D. Š.; Horvat, G.; Užarević, K.; Meštrović, E.; et al. Solid-State Chemistry and Polymorphism of the Nucleobase Adenine. *Cryst. Growth Des.* **2016**, *16*, 3262–3270.

(67)   Scudiero, L.; Barlow, D. E.; Hipps, K. W. Physical Properties and Metal Ion Specific Scanning Tunneling Microscopy Images of Metal(II) Tetraphenylporphyrins Deposited from Vapor onto Gold (111). *J. Phys. Chem. B* **2000,** *104* (50), 11899-11905.

(68)   Comanici, K.; Buchner, F.; Flechtner, K.; Lukasczyk, T.; Gottfried, J. M.; Steinruck, H. P.; Marbach, H. Understanding the Contrast Mechanism in Scanning Tunneling Microscopy (STM) Images of an Intermixed Tetraphenylporphyrin Layer on Ag(111). *Langmuir* **2008,** *24* (5), 1897-1901.

(69)   Gross, L.; Moll, N.; Mohn, F.; Curioni, A.; Meyer, G.; Hanke, F.; Persson, M. High-Resolution Molecular Orbital Imaging Using a p-Wave STM Tip. *Phys. Rev. Lett.* **2011,** *107* (8).

(70)   Ito, T.; Buhlmann, P.; Umezawa, Y. Scanning Tunneling Microscopy Using Chemically Modified Tips. *Anal. Chem.* **1998,** *70* (2), 255-259.

(71)   Nishino, T.; Buhlmann, P.; Ito, T.; Umezawa, Y. Discrimination of Functional Groups with Scanning Tunneling Microscopy Using Chemically Modified Tips: Recognition of Ether Oxygens Through Hydrogen Bond Interactions. *Phys. Chem. Chem. Phys.* **2001,** *3* (10), 1867-1869.

(72)   Ohshiro, T.; Ito, T.; Buhlmann, P.; Umezawa, Y. Scanning Tunneling Microscopy with Chemically Modified Tips: Discrimination of Porphyrin Centers Based on Metal Coordination and Hydrogen Bond Interactions. *Anal. Chem.* **2001,** *73* (5), 878-883.

(73)   van Bavel, A. P.; Hopstaken, M. J. P.; Curulla, D.; Niemantsverdriet, J. W.; Lukkien, J. J.; Hilbers, P. A. J. Quantification of Lateral Repulsion Between Coadsorbed CO and N on Rh(100) Using Temperature-Programmed Desorption, Low-Energy Electron Diffraction, and Monte Carlo Simulations. *J. Chem. Phys.* **2003,** *119* (1), 524-532.

(74)   Blunt, M. O.; Russell, J. C.; Gimenez-Lopez, M. D.; Taleb, N.; Lin, X. L.; Schroder, M.; Champness, N. R.; Beton, P. H. Guest-Induced Growth of a Surface-Based Supramolecular Bilayer. *Nature Chemistry* **2011,** *3* (1), 74-78.

(75)   Hod, I.; Sampson, M. D.; Deria, P.; Kubiak, C. P.; Farha, O. K.; Hupp, J. T. Fe-Porphyrin-Based Metal-Organic Framework Films as High-Surface Concentration,

Heterogeneous Catalysts for Electrochemical Reduction of CO_2. *ACS Catalysis* **2015,** *5* (11), 6302-6309.

(76)   Su, B.; Hatay, I.; Trojanek, A.; Samec, Z.; Khoury, T.; Gros, C. P.; Barbe, J. M.; Daina, A.; Carrupt, P. A.; Girault, H. H. Molecular Electrocatalysis for Oxygen Reduction by Cobalt Porphyrins Adsorbed at Liquid/Liquid Interfaces. *J. Am. Chem. Soc.* **2010,** *132* (8), 2655-2662.

(77)   Zagal, J. H.; Griveau, S.; Ozoemena, K. I.; Nyokong, T.; Bedioui, F., Carbon Nanotubes, Phthalocyanines and Porphyrins: Attractive Hybrid Materials for Electrocatalysis and Electroanalysis. *J. Nanosci. Nanotechno.* **2009,** *9* (4), 2201-2214.

(78)   Holten, D.; Bocian, D. F.; Lindsey, J. S. Probing Electronic Communication in Covalently Linked Multiporphyrin Arrays. A Guide to the Rational Design of Molecular Photonic Devices. *Accounts Chem. Res.* **2002,** *35* (1), 57-69.

(79)   Ambroise, A.; Wagner, R. W.; Rao, P. D.; Riggs, J. A.; Hascoat, P.; Diers, J. R.; Seth, J.; Lammi, R. K.; Bocian, D. F.; Holten, D.; et al. Design and Synthesis of Porphyrin-Based Optoelectronic Gates. *Chem. Mater.* **2001,** *13* (3), 1023-1034.

(80)   Davis, J. T. G-quartets 40 Years Later: From 5 '-GMP to Molecular Biology and Supramolecular Chemistry. *Angew. Chem. Int. Edit.* **2004,** *43* (6), 668-698.

(81)   Ciesielski, A.; Lena, S.; Masiero, S.; Spada, G. P.; Samori, P. Dynamers at the Solid-Liquid Interface: Controlling the Reversible Assembly/Reassembly Process between Two Highly Ordered Supramolecular Guanine Motifs. *Angew. Chem. Int. Edit.* **2010,** *49* (11), 1963-1966.

(82)   Lindsey, J. S. Synthetic Routes to Meso-Patterned Porphyrins. *Accounts. Chem. Res.* **2010,** *43* (2), 300-311.

(83)   Hipps, K. W.; Mazur, U. Kinetic and Thermodynamic Control in Porphyrin and Phthalocyanine Self-Assembled Monolayers. *Langmuir* **2018,** *34* (1), 3-17.

(84)   Mazur, U.; Hipps, K. W. Kinetic and Thermodynamic Processes of Organic Species at the Solution-Solid Interface: the View Through an STM. *Chem. Commun.* **2015,** *51* (23), 4737-4749.

(85)   Song, W. T.; Martsinovich, N.; Heckl, W. M.; Lackinger, M. Born-Haber Cycle for Monolayer Self-Assembly at the Liquid-Solid Interface: Assessing the Enthalpic Driving Force. *J. Am. Chem. Soc.* **2013,** *135* (39), 14854-14862.

(86)   Yokoyama, S.; Hirose, T.; Matsuda, K. Phototriggered Formation and Disappearance of Surface-Confined Self-Assembly Composed of Photochromic 2-Thienyl-Type Diarylethene: a Cooperative Model at the Liquid/Solid Interface. *Chem. Commun.* **2014,** *50* (45), 5964-5966.